https://doi.org/10.5194/egusphere-2025-4646
Preprint. Discussion started: 23 October 2025
© Author(s) 2025. CC BY 4.0 License.

Mechanistic investigations of the formation of highly oxidized products from the multi-generation OH oxidation of styrene

Long Chen,[1,2,3] Yu Huang,*[1,2,3] Yonggang Xue,[1,2,3] Long Cui,[1,2,3] Zhihui Jia[4]

[1] *State Key Laboratory of Loess Science, Institute of Earth Environment, Chinese Academy of Sciences, Xi'an 710061, China*

[2] *National Observation and Research Station of Regional Ecological Environment Change and Comprehensive Management in the Guanzhong Plain, Xi'an 710061, China*

[3] *Shaanxi Key Laboratory of Atmospheric and Haze-fog Pollution Prevention, Xi'an 710061, China*

[4] *School of Materials Science and Engineering, Shaanxi Normal University, Xi'an, Shaanxi, 710119, China*

*Corresponding author:

Prof. Yu Huang, E-mail address: huangyu@ieecas.cn

https://doi.org/10.5194/egusphere-2025-4646
Preprint. Discussion started: 23 October 2025
© Author(s) 2025. CC BY 4.0 License.

Abstract

Styrene is the second most efficient aromatic compound in the formation of secondary organic aerosol (SOA) after toluene. Recent experiments have identified C_7 and C_8 series compounds as the main components of SOA in the photooxidation of styrene. However, their molecular structures and formation pathways remain largely uncharacterized. Herein, the formation mechanisms of highly oxidized products from the multi-generation OH oxidation of styrene are studied using the quantum chemistry methods. The calculations show that the multi-generation OH oxidation mechanisms of styrene are modulated by RO_2 and RO radicals. For the first generation OH oxidation, the addition of OH radicals to the C_β-site of vinyl group is the dominant pathway, and the main C_7- and C_8-products are benzaldehyde, 1^{st}-ROOH ($C_8H_{10}O_3$) and 1^{st}-$RONO_2$ ($C_8H_9NO_3$). For the second generation OH oxidation, OH-addition reaction occurring at the *ortho*-position of 1^{st}-ROOH and 1^{st}-$RONO_2$ has a significant dominance. The peroxide bicyclic peroxy radicals (BPR) can react with $HO_2\cdot$ and NO to form the C_8-products 2^{nd}-ROOH ($C_8H_{12}O_8$) and 2^{nd}-$RONO_2$ ($C_8H_{10}N_2O_{10}$). The formed peroxide bicyclic alkoxy radical (BAR) can proceed either the ring-opening reactions to form the multifunctionalized dicarbonyls and ketene-enols, or the cyclization reactions to generate the highly oxidized C_6-epoxides with the branching ratios of ~30%. For the third generation OH oxidation, *syn*-OH-addition occurring at the C=C double bond of 2^{nd}-ROOH and 2^{nd}-$RONO_2$ has the smallest barrier. The major C_8-products are the multifunctionalized hydroperoxides and organic nitrates. The volatility of the multi-generation OH oxidation products significantly decreases with increasing the number of OH oxidation steps.

1. Introduction

Aromatic compounds are recognized as the significant secondary organic aerosol (SOA) precursors, accounting for 20%-30% of the total volatile organic compounds (VOCs) and up to ~60% of the urban atmosphere (Xu et al., 2020; Yan et al., 2019; Yu

https://doi.org/10.5194/egusphere-2025-4646
Preprint. Discussion started: 23 October 2025
© Author(s) 2025. CC BY 4.0 License.

et al., 2022; Cabrera-Perez et al., 2016; Iyer et al., 2023; Wang et al., 2017; Bloss et al., 2005; Forstner et al., 1997). The primary sources include the incomplete combustion, solvent evaporation, and industrial emission, and the secondary sources involve the biofuel and biomass burning (Xu et al., 2020; Cabrera-Perez et al., 2016; Li et al., 2019). The most abundant aromatic compounds, including benzene, toluene, ethylbenzene, xylenes, styrene and trimethylbenzenes, are highly present in urban environments (Cabrera-Perez et al., 2016; Koppmann, 2008). The degradation of aromatic compounds initiated by the atmospheric oxidants (e.g., OH radicals, NO_3 radicals, O_3, and Cl atom) leads to the formation of the highly oxidized products (e.g., nitroaromatics, dicarbonyls, cresols, epoxides) (Ji et al., 2017; Wu et al., 2014; Fu et al., 2023; Wang and Li, 2021; Wang et al., 2013; Zaytsev et al., 2019; Wang et al., 2020), significantly contributing to new particle formation (NPF) and SOA formation (up to 50% in eastern China) in the atmosphere (Wang et al., 2017; Wang et al., 2020; Garmash et al., 2020; Molteni et al., 2018; Nie et al., 2022).

Styrene has been identified as the second most efficient aromatic compound in the formation of SOA after toluene (Sun et al., 2016; Tajuelo et al., 2019a), which is primarily emitted from the anthropogenic activities such as solvent usage and vehicle exhaust (Cho et al., 2014; Wu et al., 2021). Styrene is detected at the ppb levels in urban environments, with the mixing ratios of 0.06-4.50 ppb (Cho et al., 2014; Huang et al., 2019), which has been classified as a hazardous air pollutant in the 1990 Clean Air Act due to the potential mutagen and carcinogen (Environmental Protection Agency (EPA), 1990). Therefore, it is very necessary to investigate the degradation mechanisms of styrene under atmospheric conditions. In general, the atmospheric oxidation of styrene initiated by OH radicals is anticipated to be the dominant daytime sink, and the lifetime is estimated to be ~ 8 h under the conditions of typical OH radicals concentrations ([OH] = ~ 2 × 10^6 molecules cm^{-3}) (Wu et al., 2021; Shen et al., 2022). Due to the existence of highly reactive vinyl and aromatic groups, OH-initiated oxidation of styrene mainly comprise two kinds of pathways: H-abstraction and OH-addition, in which C_β-site OH-addition reaction is expected to be the predominant pathway (Wu et al., 2021; Wang et al., 2015; Zhang et al., 2024).

https://doi.org/10.5194/egusphere-2025-4646
Preprint. Discussion started: 23 October 2025
© Author(s) 2025. CC BY 4.0 License.

The formed products can combine with an O_2 molecule leading to the first generation peroxyl radicals, which can further react with NO resulting in the formation of benzaldehyde and formaldehyde. The barrier of the rate-limiting step is predicted to be 28.4 kcal/mol (Wang et al., 2015), implying that benzaldehyde is unlikely to be the sole primary product in the oxidation of styrene due to their higher barriers. Additionally, carbonyl oxides, formed in the ozonolysis of styrene, serve as the chain units participating in the formation of oligomers (Yu et al., 2022). The volatility of oligomers decreases dramatically as the successive addition of carbonyl oxides increases, eventually transforming into extremely low volatility organic compounds (ELVOC) and directly participating in NPF.

Experimentally, Cho et al., (2014) investigated the kinetics of the reaction styrene + ·OH at 240-340 K and 1-3 Torr using the mass spectrometry technique. They found that the addition of OH radicals to the vinyl carbons is dominant, and the determined rate coefficient is $(5.80 \pm 0.49) \times 10^{-11}$ cm^3 $molecule^{-1}$ s^{-1} at room temperature. In the smog chamber experiments, Tajuelo et al., (2019a, 2019b and 2019c) found that the SOA yields from the photolysis and photooxidation of styrene and its homologous species increase with the concentration of initial reactants increasing, and benzaldehyde, benzoyl chloride, acetophenone and formaldehyde are expected to be the primary gas phase products. Yu et al., (2022) investigated the formation of SOA from styrene in an indoor chamber under different NO_x and RH conditions, and found the SOA yields decrease with increasing RH in both the H_2O_2 and NO_x systems. The C_7 and C_8 species are the main products in the H_2O_2 system, while organic nitrates are the major components in the NO_x system. Although the possible molecular formula and chemical composition of the oxidation products from the reaction styrene + ·OH are given in the aforementioned studies, the specific molecular structures and formation pathways remain ambiguous. Additionally, to the best of our knowledge, the majority of studies mainly focus on the first generation OH oxidation products to date, while the formation mechanisms of highly oxidized products from the multi-generation ·OH oxidation of styrene are still limited.

In the present study, the multi-generation ·OH oxidation mechanisms of styrene

https://doi.org/10.5194/egusphere-2025-4646
Preprint. Discussion started: 23 October 2025
© Author(s) 2025. CC BY 4.0 License.

in the presence of HO_2 /NO are investigated using the quantum chemistry methods. The calculated results arising from the first generation OH oxidation reactions are presented herein for comparison with the available literatures to ascertain the reliability of the employed theoretical method. For the multi-generation OH oxidation reactions of styrene, all the possible pathways, including OH-addition, O_2-addition, cyclization, ring-opening, intramolecular H-shifts, C-C bond scission, and HO_2-elimination reactions, are taken into account. Additionally, the saturated concentrations of the formed highly oxidized products are estimated to identify their volatility classes.

2. Computational methods

2.1 Electronic structures and energy calculations

The electronic structures and energy calculations of all stationary points, including reactants (R), intermediates (IM), transition states (TS) and products (P), are performed using the Gaussian 16 program (Frisch et al., 2016). Geometric optimizations of all stationary points on the potential energy surfaces (PESs) are carried out at the M06-2X/6-31+g(d,p) level of theory, since it has reliable performance for describing the noncovalent interactions, thermochemical, and kinetics (Zhao and Truhlar, 2008). Harmonic vibrational frequencies are determined at the M06-2X/6-31+g(d,p) theoretical level to confirm the characteristics of all stationary points (a local minimum or a saddle point). The zero-point vibrational energy (ZPVE) is scaled by a factor of 0.967 (Alecu et al., 2010). Intrinsic reaction coordinate (IRC) calculations are carried out to ascertain the connection of the given TS between the designated local minima R and P (Fukui, 1981). Single point energy calculations are performed at the M06-2X/6-311++G(3df,3pd) level of theory, which has been demonstrated to yield accurate energetics compared to that of the gold standard methods (e.g., QCISD(T), CCSD(T) and ROHF-ROCCSD(T)-F12a) (Ji et al., 2018; Fu et al., 2024). The activation energy (ΔE_a) and reaction energy (ΔE_r) are defined as the difference in energy between TS and R, as well as between P and R.

2.2 Conformer search

https://doi.org/10.5194/egusphere-2025-4646
Preprint. Discussion started: 23 October 2025
© Author(s) 2025. CC BY 4.0 License.

RO_2 radicals, formed in the addition of O_2 to the carbon-centered site of alkyl radicals, have multiple conformers due to the varying attack directions of O_2 (Chen et al., 2021; Fu et al., 2020; Møller et al., 2020). In order to obtain the stable conformer of RO_2 radicals, the conformer search is conducted using the Molclus program (Lu, 2024). For the intramolecular H-shift reactions of RO_2 radicals, the B3LYP/6-31+g(d) optimized structures of R, TS and P are selected as the initial geometries to perform the conformational sampling. Notably, the cyclic TS structure in the conformational sampling of TSs is constrained by adjusting the lengths of the O-O, C-H and O-H bonds in RO_2 radicals. Next, the resulting structures are initially optimized at the same level, since it has been demonstrated to be effective in determining the relative energies of various conformers (Rissanen et al., 2014; Hyttinen et al., 2015). The conformers within 2.0 kcal/mol with respect to the lowest energy conformer are further optimized at the M06-2X/6-31+g(d,p) level of theory. Then, the single point energy calculations are performed at the M06-2X/6-311++G(3df,3pd) level of theory. Similar methodology is adopted to investigate the isomerization reactions of RO radicals.

2.3 Kinetics calculations

The rate coefficients of unimolecular reactions, such as intramolecular H-shift and the cyclization of RO_2 and RO radicals, are calculated using the RRKM theory along with energy-grained master equation (RRKM-ME) (Holbrook et al., 1996), while the rate coefficients of bimolecular reactions, such as OH-addition and HO_2-elimination, are determined using the traditional transition state theory (TST) (Fernández-Ramos et al., 2007). An asymmetric one-dimensional Eckart model (Eckart, 1930) is taken into consideration for the tunneling correction factors in the rate coefficient calculations of RRKM-ME and TST. A single exponential down model in the RRKM-ME calculations is utilized to approximate the collision transfer ($\langle \Delta E \rangle_{down}$ = 200 cm^{-1}). The Lennard-Jones parameters of all intermediate species are estimated using the empirical formula as proposed by Gilbert and Smith (1990).

For the intramolecular H-shifts of RO_2 and RO radicals, the rate coefficients are

https://doi.org/10.5194/egusphere-2025-4646
Preprint. Discussion started: 23 October 2025
© Author(s) 2025. CC BY 4.0 License.

computed using the multiconformer transition state theory (MC-TST) (Møller et al., 2016), which is expressed as Eq. (1): (Møller et al., 2016 and 2020; Pasik et al., 2024)

$$k_{\text{MC-TST}} = \kappa \frac{k_B T}{h} \frac{\sum_i^{\text{TS conf.}} \exp(\frac{-\Delta E_i}{k_B T}) Q_{\text{TS},i}}{\sum_j^{\text{R conf.}} \exp(\frac{-\Delta E_j}{k_B T}) Q_{\text{R},j}} \exp\left(-\frac{E_{\text{TS}} - E_{\text{R}}}{k_B T}\right) \quad (1)$$

where κ is the Eckart tunneling coefficient, h is Planck's constant, k_B is Boltzmann's constant, and T is the absolute temperature (298.15 K). $Q_{\text{TS},i}$ and $Q_{\text{R},j}$ refer to the partition functions of the corresponding transition state i and reactant j conformers, respectively. ΔE_i and ΔE_j represent the relative electronic energies between the corresponding transition state i and reactant j conformers and the lowest energy conformers, respectively. E_{TS} and E_{R} stand for the electronic energies of the lowest energy transition state and reactant conformers, respectively. All kinetics calculations are carried out using the KiSThelP 2021 and MESMER 6.0 programs (Glowacki et al., 2012; Canneaux et al., 2013).

3. Results and discussion

3.1 First generation ·OH oxidation mechanisms of styrene

Styrene is composed of a benzene ring and a vinyl group, and its oxidation initiated by OH radicals may proceed either on the vinyl group or on the benzene ring. Previous literature has demonstrated that the addition of OH radicals to terminal carbon (C_β-site) of a vinyl group in styrene is the dominant pathway, with the branching ratio of 88.2% (Wu et al., 2021). Therefore, the C_β-site OH-addition reaction is mainly considered in the present study. Figure 1 depicts that this reaction starts with the formation of a pre-reactive complex IM1, and then transforms into an alkyl radical S1-1 via transition state TS1 with the apparent barrier and activation barrier of -3.5 and 0.8 kcal/mol. The calculated results are in good agreement with the values of -2.6 and 0.6 kcal/mol predicted at the high theoretical level DLPNO-CCSD(T)//M06-2X (Wu et al., 2021; Zhang et al., 2024). The rate coefficient of C_β-site OH-addition reaction is estimated to be 1.5×10^{-11} cm^3 $molecule^{-1}$ s^{-1} at ambient temperature, which is approximately consistent with the

https://doi.org/10.5194/egusphere-2025-4646
Preprint. Discussion started: 23 October 2025
© Author(s) 2025. CC BY 4.0 License.

experimental (1.2-6.2 × 10^{-11} cm^3 $molecule^{-1}$ s^{-1}) and theoretical values (1.7-2.0 × 10^{-11} cm^3 $molecule^{-1}$ s^{-1}) for the total rate coefficient of the reaction styrene + OH (Wu et al., 2021; Zhang et al., 2024)]. The aforementioned results reveal that the computational method employed herein is reasonable to describe the atmospheric oxidation mechanisms of styrene.

Due to the existence of resonance structures with radical character on the aromatic ring, the resulting S1-1 can readily isomerize into three other species, namely, S1-2, S1-3 and S1-4. Next, S1-1 can combine with an O_2 molecule leading to the formation of first generation peroxy radicals S2-1-x (ΔE_r > 59.6 kcal/mol), which includes eight energetically similar conformers, and the corresponding Boltzmann population is listed in Table S1. Notably, the formations of peroxy radicals S2-2-x from the association reactions S1-2 + O_2 are strongly endothermic (ΔE_r = 8.1-10.4 kcal/mol), as depicted in Figure S1, suggesting that they have a significant potential to redissociate back to S1-2 and O_2. The resulting S2-2-x can undergo through various intramolecular H-shifts to yield distinct C-centered and O-centered radicals. Among these competing H-shift pathways, hydrogen transfer from the –OH group to the terminal oxygen of –OO group has the lowest barrier (ΔE_a = 17.4 kcal/mol). A similar conclusion is also obtained from the association reactions S1-3 + O_2 (ΔE_r = 6.6-7.1 kcal/mol) and S1-4 + O_2 (ΔE_r = 8.1-11.1 kcal/mol) that the formations of RO_2 radicals are unfavorable thermochemically (Figures S2 and S3). Therefore, in the present study, we mainly focus on the subsequent reaction mechanisms of peroxy radicals S2-1-x under both low and high NO_x conditions.

For the unimolecular reactions of S2-1-x, there are three kinds of pathways. One is the H-shift reactions, where the hydrogen atom migrates from the –CH_2, –CH and –OH groups to the terminal oxygen atom of the –OO group leading to QOOH radicals. Among these competing H-shift reactions, the hydrogen atom transfer from the –OH group to the –OO group proceeds via a five-membered ring transition state to yield a hydroperoxyalkoxy radical S3-1-a, which exhibits the smallest barrier (ΔE_a = 21.0 kcal/mol). Then, the decomposition of S3-1-a undergoes through the successive elimination of HCHO and an OH radical to generate benzaldehyde. Based on the

https://doi.org/10.5194/egusphere-2025-4646
Preprint. Discussion started: 23 October 2025
© Author(s) 2025. CC BY 4.0 License.

values of ΔE_a, it can be concluded that H-shift reaction is the rate-determining step in the whole process. The other is the intramolecular cyclization, where the –OO group attacks the C=C double bond in the benzene ring forming a cyclic peroxide alkyl radical S3-1-c (ΔE_a = 33.6 kcal/mol). The last is the HO_2-elimination reaction, where a concerted process of C_α-O and C_β-H bonds scission forms a closed-shell species S3-1-b and a HO_2 radical byproduct (ΔE_a = 33.3 kcal/mol). The aforementioned results show that the cyclization and HO_2-eliminaiton reactions are less importance due to their higher barriers. The rate coefficient of the unimolecular reactions of S2-1-x is calculated to be 1.6×10^{-4} s^{-1} at room temperature, which is about two orders of magnitude lower than the typical pseudo-first-order rate constants $k'_{RO2+HO2}$ (~ 0.01 s^{-1}) and k'_{RO2+NO} (~ 0.01 s^{-1}) of the bimolecular reactions of RO_2 radicals with HO_2 radicals and NO (Fu et al., 2024; Pasik et al., 2024).

In the presence of NO, the bimolecular reactions of S2-1-x with NO proceed via oxygen-to-oxygen coupling to generate organic nitrites ROONO, followed by decomposition to benzaldehyde and CH_2OH radical or isomerization to organic nitrates $RONO_2$. Wang et al. predicted that the energy barrier of the rate-limiting step for the formation of benzaldehyde is 28.4 kcal/mol, which is approximately 4.0 kcal/mol greater than that of the formation of $RONO_2$ (Wang et al., 2015). Moreover, reactions with HO_2 radicals leading to hydroperoxides ROOH are anticipated to be one of the dominant sinks for S2-1-x under low NO_x conditions. Specifically, SOA yields obtained from the reaction $RO_2 \cdot + HO_2 \cdot \rightarrow$ ROOH under low NO_x conditions are greater than those derived from the reaction $RO_2 \cdot + NO \rightarrow RONO_2$ under high NO_x conditions for some aromatic compounds (e.g, m-xylene, toluene) (Ng et al., 2007). The aforementioned results imply that ROOH and $RONO_2$ may be significant oxidation products expect benzaldehyde in the photooxidation of styrene. The hypothesis is further confirmed by the recent smog chamber experiment study that C_7 and C_8 series products, as well as organic nitrates are the main components of SOA in the OH-initiated oxidation of styrene under different NO_x conditions (Yu et al., 2022). Considering that the extensive studies on the oxidation of benzaldehyde have done (Sebbar et al., 2011; Zhao et al., 2022; Iuga et al., 2008), this study primarily focus on

https://doi.org/10.5194/egusphere-2025-4646
Preprint. Discussion started: 23 October 2025
© Author(s) 2025. CC BY 4.0 License.

the multi-generation ·OH oxidation mechanisms of ROOH and $RONO_2$ under different NO_x conditions.

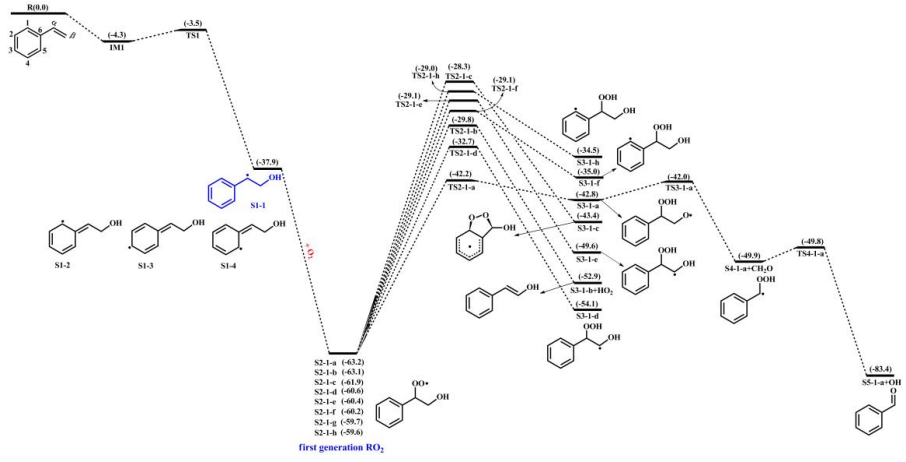

Figure 1. PES for the first-stage oxidation of styrene initiated by OH radicals and the unimolecular reactions of S2-1-x at the M06-2X/6-311++G(3df,3pd)//M06-2X/6-31+g(d,p) level

3.2 Second generation ·OH oxidation mechanisms of 1st-ROOH and 1st-$RONO_2$

The first generation products, including hydroperoxides 1st-ROOH and organic nitrates 1st-$RONO_2$, include multiple conformers. To obtain the global minimum of 1st-ROOH and 1st-$RONO_2$, the conformer search is performed by using the Molclus program. The resulting structures are initially optimized at the M06-2X/6-31+g(d,p) level, then the single point energies are calculated at the M06-2X/6-311++G(3df,3pd) level. The global minimum structures of 1st-ROOH (S4) and 1st-$RONO_2$ (S5) are presented in Figure S4.

3.2.1 The oxidation mechanism of 1st-ROOH initiated by OH radicals

The reaction 1st-ROOH (S4) + ·OH proceeds through the addition of OH radicals to either side of the benzene ring to yield alkyl radicals, as depicted in Figure 2. Based on the values of ΔE_a, OH-addition occurring at the opposite direction of –OOH group exhibit significantly lower barriers compared to that at the same direction of –OOH group. This discrepancy in barrier heights could be attributed to the existence of large

https://doi.org/10.5194/egusphere-2025-4646
Preprint. Discussion started: 23 October 2025
© Author(s) 2025. CC BY 4.0 License.

steric hindrance in the latter case. Among all the OH-addition reactions occurring at the opposite direction of –OOH group, the addition of OH radicals to C_1-site has the smallest barrier ($R_{S4\text{-}add1}$, ΔE_a = 0.8 kcal/mol) due to the stability of $P_{S4\text{-}add1}$. The result is opposite to Zhang's finding that the addition of OH radicals to C6-site would be the most favorable pathway (Zhang et al., 2024). The difference in the preferred pathways can be attributed to the absence of the pre-reactive complexes in Zhang's study, leading to potentially incorrect conclusions. Our result is further supported by the analogous reaction systems, such as the reaction toluene + OH, that the *ortho*-addition reaction has a significant dominance (Ji et al., 2017; Wu et al., 2014; Zhang et al., 209; Wu et al., 2020).

$P_{S4\text{-}add1}$ includes two conjugate double bonds (C_2=C_3 and C_4=C_5), which can readily isomerize to $P_{S4\text{-}add1'}$ and $P_{S4\text{-}add1''}$, as evident from Figure S5. In the present of O_2, the attack of an O_2 molecule on the C-centered site of $P_{S4\text{-}add1}$, $P_{S4\text{-}add1'}$, and $P_{S4\text{-}add1''}$ proceed via the barrierless processes to produce the second generation peroxy radicals $P_{S4\text{-}add1}$-OO, $P_{S4\text{-}add1'}$-OO and $P_{S4\text{-}add1''}$-OO. The O_2-addition reaction occurring at the same direction as the –OOH group is defined as *syn*-O_2-addition, while the O_2-addition reaction occurring at the opposite direction as the –OOH group is defined as *anti*-O_2-addition. For the reaction $P_{S4\text{-}add1}$ + O_2 → $P_{S4\text{-}add1}$-OO-a/-s, ΔE_r of *anti*-O_2-addition is -5.8 kcal/mol, which is lower than that of *syn*-O_2-addition by 0.4 kcal/mol, suggesting that *anti*-O_2-addition is preferable over *syn*-O_2-addition in energy. For the reactions $P_{S4\text{-}add1'}$ + O_2 → $P_{S4\text{-}add1'}$-OO-a/-s and $P_{S4\text{-}add1''}$ + O_2 → $P_{S4\text{-}add1''}$-OO-a/-s, it can be concluded the same by the values of ΔE_r that *anti*-O_2-addition reaction is energetically feasible.

The resulting $P_{S4\text{-}add1}$-OO can proceed intramolecular cyclization reaction, where the attack of end-site oxygen atom of the –OO group on C_2-site of the C_2=C_3 double bond, leading to the formation of peroxide bicyclic alkyl radicals. ΔE_a and ΔE_r of the reaction $P_{S4\text{-}add1}$-OO-a → $P_{S4\text{-}add1}$-OO-a-1 are 11.8 and -16.8 kcal/mol, respectively, which are lower than those of the reaction $P_{S4\text{-}add1}$-OO-s → $P_{S4\text{-}add1}$-OO-s-1 by 3.9 and 2.2 kcal/mol, respectively. The aforementioned results reveal that the intramolecular cyclization reaction of *anti*-O_2-addition product $P_{S4\text{-}add1}$-OO-a is favorable on both

https://doi.org/10.5194/egusphere-2025-4646
Preprint. Discussion started: 23 October 2025
© Author(s) 2025. CC BY 4.0 License.

thermochemically and kinetically. A similar conclusion is also derived from the intramolecular cyclization reactions of *anti*-O_2-addition products $P_{S4\text{-}add1''}$-OO-a and $P_{S4\text{-}add1''}$-OO-a. Notably, the barriers of the intramolecular cyclization reactions $P_{S4\text{-}add1''}$-OO-a → $P_{S4\text{-}add1''}$-OO-a-1 (ΔE_a = 31.1 kcal/mol) and $P_{S4\text{-}add1''}$-OO-a → $P_{S4\text{-}add1''}$-OO-a-2 (ΔE_a = 34.6 kcal/mol) are extremely high, making them insignificant in the atmosphere. The tautomerization between $P_{S4\text{-}add1}$-OO-a-1 and $P_{S4\text{-}add1''}$-OO-a-1 readily occurs due to the existence of resonance structures, and it is therefore that the latter conformer is selected as a prototype for the investigating of its subsequent reaction mechanism.

The formed $P_{S4\text{-}add1''}$-OO-a-1 can combine with an O_2 molecule leading to the third generation peroxy radicals (also called as peroxide bicyclic peroxy radicals, BPR) $P_{S4\text{-}add1''}$-OO-a-2, and the lowest energy conformer is presented in Figure S6. The isomerization of $P_{S4\text{-}add1''}$-OO-a-2 may undergo through a concerted process of the cleavage of -O-O- bridge bond and C_1-C_2 bond as well as hydrogen atom transfer from the hydroxyl group to the bridge oxygen atom, yielding a new peroxy radical (ΔE_a = 28.5 kcal/mol). The room temperature rate coefficient is calculated to be 3.0×10^{-9} s^{-1}, which is several orders of magnitude low than the typical pseudo-first-order rate constants $k'_{RO2+HO2}$ (~ 0.01 s^{-1}) and k'_{RO2+NO} (~ 0.01 s^{-1}), suggesting that the isomerization reaction is insignificance in the atmosphere. Therefore, the bimolecular reactions of $P_{S4\text{-}add1''}$-OO-a-2 are mainly taken into consideration in this study.

In the pristine environments, $P_{S4\text{-}add1''}$-OO-a-2 can react with HO_2 radicals resulting in the formation of the second generation products, bicyclic hydroperoxide 2^{nd}-ROOH (S6) and peroxide bicyclic alkoxy radical (BAR) $P_{S4\text{-}add1''}$-OO-a-3, as depicted in Figure S6. For the subsequent reactions of S6 initiated by OH radicals, the detailed mechanisms are discussed in Section 3.3.1. From Figure 3, it can be seen that the unimolecular decomposition of $P_{S4\text{-}add1''}$-OO-a-3 involves two kinds of pathways. One is the ring-opening reaction, where the breakage of C_5-C_6 bond produces an alkyl radical S7 (ΔE_a = 5.9 kcal/mol,). The other is cyclization reaction, where the attack of oxygen atom of O-centered site on the C_4-site of the C_3=C_4 double bond generates the ring-retaining alkyl radical S15 (E_a = 8.0 kcal/mol). The branching ratios for the

https://doi.org/10.5194/egusphere-2025-4646
Preprint. Discussion started: 23 October 2025
© Author(s) 2025. CC BY 4.0 License.

formation of S7 and S15 are predicted to be 74.7% and 25.3%, respectively.

As shown in Figure 3, S7 decomposes through the barrierless rupture of -O-O- bridge bond to form alkoxy radical S8-x, which includes five possible conformers as presented in Figure S7. The Boltzmann populations of different conformers are listed in Table S2. S8-x can undergo intramolecular H-shifts, in which a hydrogen atom is transferred from different carbon atoms to O-centered site, forming the alkyl radicals. Among the competing H-shift reactions, 1,5 H-shift occurring at the $-C_5(O)H$ group exhibits the smallest barrier (ΔE_a = 0.6 kcal/mol), and $k_{MC\text{-}TST}$ is calculated to be 8.2 × 10^9 s^{-1} at ambient temperature (Table S3). The formed S8-e-P can readily isomerize to S9 due to its resonance stabilized structure, followed by decomposition into a ketene-enol S10 and an alkyl radical S11 (ΔE_a = 16.1 kcal/mol), or dissociation to S13 and CO (ΔE_a = 29.4 kcal/mol). S11 can further react with O_2 leading to a HO_2 radical and a hydroperoxide S12 that possessed a hydroxyl and two carbonyl groups (ΔE_a = 14.0 kcal/mol). Alternatively, S8-x can proceed through the C_1-C_2 bond scission to yield an unsaturated 1,4-dicarbonyl species S14 and an alkyl radical S11 (ΔE_a = 2.2 kcal/mol), with the rate coefficient of 2.1 × 10^{10} s^{-1}. Notably, both the 1,5 aldehyde H-shift and C_1-C_2 bond scission reactions yield a closed-shell species S12 with up to five oxygen atoms, and the branching ratios are predicted to be 28.1% and 71.9%, respectively. The result is further supported by the previous study that the proportion of aldehyde H-shift products constitutes about one third of the total products in the reaction benzene + ·OH (Wang et al., 2020).

As shown in Figure 3, S15 can further react with O_2 leading to the fourth generation peroxy radical S16-x, which can proceed either intramolecular H-shifts forming QOOH (Figure S8), or reactions with RO_2 radicals forming alkoxyl radical S17. Notably, the barriers of intramolecular H-shifts are significantly high (ΔE_a > 34.6 kcal/mol), making them less importance in the atmosphere. The transformation of S17 undergoes through the breakage of C_2-C_3 bond to produce S18 (ΔE_a = 9.4 kcal/mol), followed by fragmentation into an alkoxyl radical S19 via the barrierless rupture of the -O-O- bridge bond. Then, S19 dissociates to an OH radical, a glycolaldehyde S25 and a C_6-epoxide product S23 bearing a hydroxy and three carbonyl groups, being the

https://doi.org/10.5194/egusphere-2025-4646
Preprint. Discussion started: 23 October 2025
© Author(s) 2025. CC BY 4.0 License.

dominant pathway. The regeneration of OH radicals drives the successive autoxidation of styrene, eventually leading to the formation of the highly oxidized products.

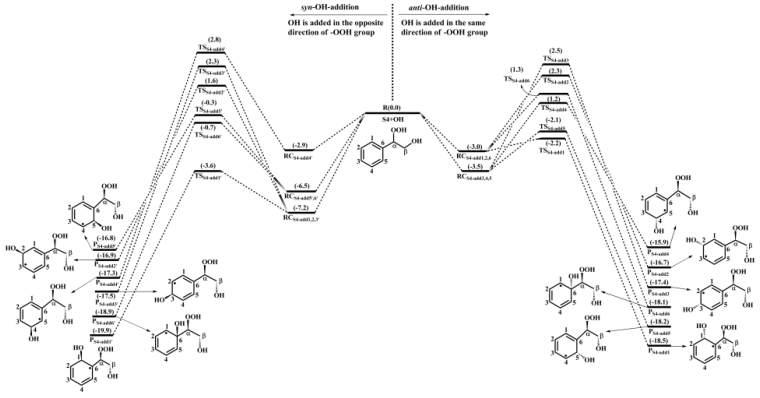

Figure 2. PES for the oxidation of 1st-ROOH(S4) initiated by OH radicals at the M06-2X/6-311++G(3df,3pd)//M06-2X/6-31+g(d,p) level

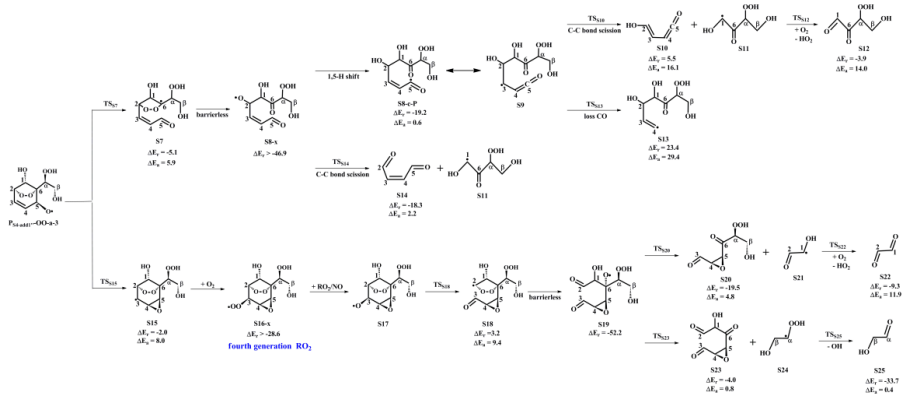

Figure 3. PES for the unimolecular decomposition of $P_{S4\text{-}add1''}$-OO-a-3 and its subsequent reactions at the M06-2X/6-311++G(3df,3pd)//M06-2X/6-31+g(d,p) level

3.2.2 The oxidation mechanism of 1st-$RONO_2$ initiated by OH radicals

The OH-initiated oxidation of 1st-$RONO_2$ (S5) proceeds through the addition of OH radicals to different carbon sites in the benzene ring to form various alkyl radicals $P_{S5\text{-}addx}$, as depicted in Figure 4. Among the competing OH-addition reactions, the OH-addition reaction at the C1-site, which proceeds in the opposite direction as the –ONO_2 group, has the smallest barrier ($R_{S5\text{-}add1}$, ΔE_a = 0.4 kcal/mol) due to the stability

https://doi.org/10.5194/egusphere-2025-4646
Preprint. Discussion started: 23 October 2025
© Author(s) 2025. CC BY 4.0 License.

of the formed product $P_{S5\text{-}add1}$. The result again shows that the *ortho*-addition reaction is energetically feasible. $P_{S5\text{-}add1}$ may isomerize to two other resonance structures, namely, $P_{S5\text{-}add1'}$ and $P_{S5\text{-}add1''}$. For the reaction $P_{S5\text{-}add1}$ + O_2, O_2 may add on either the opposite (*anti*-O_2-addition) or the same direction (*syn*-O_2-addition) relative to the –NO_3 group, leading to the second generation peroxyl radicals $P_{S5\text{-}add1}$-OO-a and $P_{S5\text{-}add1}$-OO-s (Figure S9). The exoergicity of these two reactions are 6.7 and 4.4 kcal/mol, respectively, suggesting that the *anti*-O_2-addition reaction is thermochemically favorable. Next, they can isomerize via a cyclization process to yield $P_{S5\text{-}add1}$-OO-a-1 and $P_{S5\text{-}add1}$-OO-s-1 with the ΔE_a of 13.3 and 18.1 kcal/mol. This result shows that the cyclization reaction of *anti*-O_2-addition product $P_{S5\text{-}add1}$-OO-a is kinetically feasible. A similar conclusion is also obtained from the reaction $P_{S5\text{-}add1''}$ + O_2 that the formation of *anti*-O_2-addition product $P_{S5\text{-}add1''}$-OO-a-1 is dominant. Due to the existence of the conjugate double bond, it facilitates the tautomerization between $P_{S5\text{-}add1}$-OO-a-1 and $P_{S5\text{-}add1''}$-OO-a-1. Therefore, we mainly focus on the subsequent chemistry of $P_{S5\text{-}add1''}$-OO-a-1 in the present study.

$P_{S5\text{-}add1''}$-OO-a-1 can further react with an O_2 molecule leading to the third generation peroxyl radicals $P_{S5\text{-}add1''}$-OO-a-2, which include multiple conformers. The lowest energy conformer resulting from conformer search is presented in Figure S10. In urban environments, the bimolecular reaction of $P_{S5\text{-}add1''}$-OO-a-2 with NO yields the second generation products, bicyclic organic nitrate 2^{nd}-$RONO_2$ (S26) and BAR $P_{S5\text{-}add1''}$-OO-a-3 as displayed in Figure S10. The detailed mechanism of OH-initiated oxidation of S26 is discussed in Section 3.3.2. As shown in Figure 5, $P_{S5\text{-}add1''}$-OO-a-3 can either proceed via a ring opening process to form an alkyl radical S27 (ΔE_a = 7.3 kcal/mol), or undergo through a cyclization process to generate an epoxide species S35 (ΔE_a = 8.5 kcal/mol). The branching ratios of these two reactions are predicted to be 69.2% and 30.8%, respectively. Notably, the branching ratio of cyclization reaction of $P_{S5\text{-}add1''}$-OO-a-3 increases by 5.5% compared to that of cyclization reaction of $P_{S4\text{-}add1''}$-OO-a-3, suggesting that the –ONO_2 substitution is beneficial to cyclization reaction.

The degradation of S27 proceeds through the barrierless scission of -O-O- bridge

https://doi.org/10.5194/egusphere-2025-4646
Preprint. Discussion started: 23 October 2025
© Author(s) 2025. CC BY 4.0 License.

bond to form S28-x, and the Boltzmann populations of different conformers are listed in Table S4. S28-x can undergo via various intramolecular H-shifts to produce QOOH, in which hydrogen atom transfer from the –C(O)H group to the terminal oxygen atom has the smallest barrier (ΔE_a = 2.0 kcal/mol). Alternatively, S28-x can proceed through the cleavage of C_1-C_2 bond to generate an unsaturated 1,4-dicarbonyl compound S34 and an alkyl radical S31 (Figure S11). The rare coefficients of these two pathways are predicted to be 1.7×10^9 and 5.8×10^9 s^{-1} (Table S5), respectively, with the branching ratios of 23% and 77%. The formed S31 may undergo through H-abstraction by O_2 to yield an organic nitrate S32 bearing a hydroxyl and two carbonyl groups (ΔE_a = 11.7 kcal/mol).

S35 can combine with an O_2 molecule forming the fourth generation peroxyl radicals S36-x, which have five possible conformers. S36-x can proceed either intramolecular H-shifts forming QOOH, or reaction with RO_2 radicals generating alkoxyl radical S37. However, the barriers of intramolecular H-shifts are extremely high (ΔE_a > 31.3 kcal/mol), making them less importance in the atmosphere (Figure S12). The degradation of S37 initially proceeds via the breakage of C_2-C_3 bond to form S38 (ΔE_a = 9.2 kcal/mol), followed by decomposition into an alkoxyl radical S39 via the barrierless scission of -O-O- bridge bond. The dominant pathway of the unimolecular decomposition of S39 is the formation of a glyoxal and a C_6-epoxide species S40-1 bearing a $–NO_3$, a hydroxyl and two carbonyl groups. This process differs from the unimolecular decay of S19, where the favorable pathways is the formation of a tricarbonyl compound S23. The aforementioned results reveal that the preferable pathway is strongly dependent on the breakage of C-C bond associated with the property of substituents in the decomposition of alkoxy radicals.

https://doi.org/10.5194/egusphere-2025-4646
Preprint. Discussion started: 23 October 2025
© Author(s) 2025. CC BY 4.0 License.

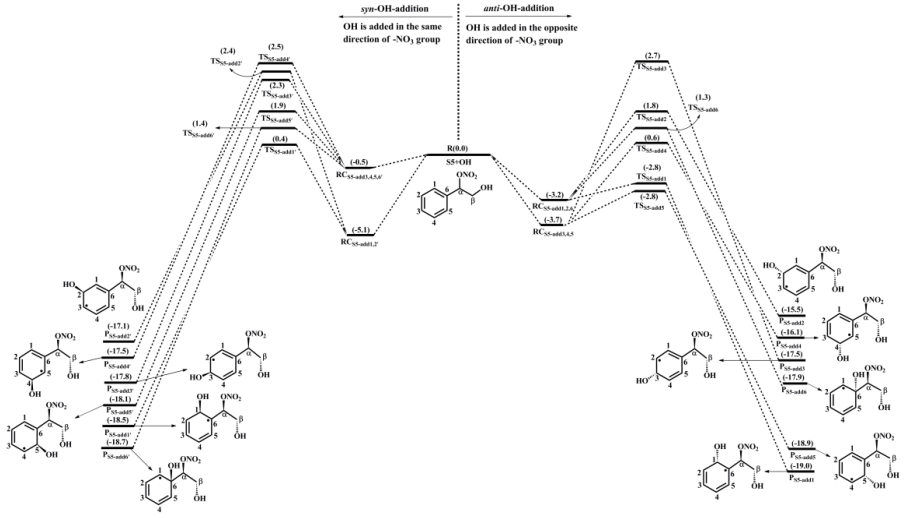

Figure 4. PES for the oxidation of 1st-$RONO_2$(S5) initiated by OH radicals at the M06-2X/6-311++G(3df,3pd)//M06-2X/6-31+g(d,p) level

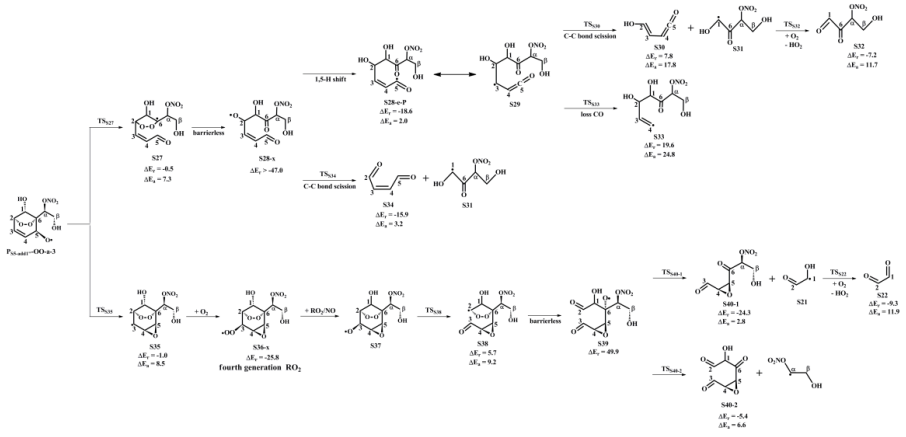

Figure 5. PES for the unimolecular decomposition of $P_{S5\text{-}add1^n}$-OO-a-3 and its subsequent reactions at the M06-2X/6-311++G(3df,3pd)//M06-2X/6-31+g(d,p) level

3.3 Third generation ·OH oxidation mechanisms of 2nd-ROOH and 2nd-$RONO_2$

The second generation products, bicyclic hydroperoxide 2nd-ROOH and bicyclic organic nitrate 2nd-$RONO_2$, have multiple conformers. The global minimum structures of 2nd-ROOH (S6) and 2nd-$RONO_2$ (S26) resulting from the conformer search are presented in Figures S6 and S10, respectively.

3.3.1 The oxidation mechanism of 2nd-ROOH initiated by OH

https://doi.org/10.5194/egusphere-2025-4646
Preprint. Discussion started: 23 October 2025
© Author(s) 2025. CC BY 4.0 License.

radicals

OH-initiated oxidation of 2nd-ROOH (S6) undergoes through the addition of OH radicals to either side of the C_3=C_4 double bond to generate the alkyl radicals. In this context, *syn*-OH-addition is defined as the scenario in which the addition of OH radicals occurs at the same side as the –OOH group, while *anti*-OH-addition is referred to the scenario in which the addition of OH radicals occurs at the opposite side as the –OOH group. As shown in Figure S13, the *syn*-OH-addition occurring at the C_3-site in the C_3=C_4 double bond has the smallest barrier (ΔE_a = 2.4 kcal/mol). Next, the unimolecular decay of *syn*-OH-addition product $P_{S6\text{-}add3}$ proceeds through a cyclization process to yield an epoxide compound S41 and an OH radical byproduct (ΔE_a = 15.3 kcal/mol), or undergoes via intramolecular 1,4 H-shift to form a peroxy radical S42 (ΔE_a = 21.8 kcal/mol), or proceeds via the elimination of hydrogen atom to produce an alkene S43 (ΔE_a = 37.9 kcal/mol), as depicted in Figure S14. Based on the values of ΔE_a, the dominant pathway of the unimolecular decomposition of $P_{S6\text{-}add3}$ is the formation of S41, and the rate coefficient k_{R41} is calculated to be 1.8×10^2 s^{-1}. The pseudo-first-order rate constant k'_{R+O2} of the bimolecular reactions of typical alkyl radicals with O_2 is 3.0×10^7 s^{-1} (Ma et al., 2021), which is about five orders of magnitude greater than k_{R41}, suggesting that the unimolecular decomposition of $P_{S6\text{-}add3}$ is insignificant.

As shown in Figure 6, the fourth generation peroxy radicals S44-x formed in the addition reaction $P_{S6\text{-}add3}$ + O_2 can either proceed via intramolecular H-shits to form QOOH, or undergo through self- or cross-reactions to yield an alkoxy radical S45. Due to the considerably high barriers of intramolecular H-shifts, they are deemed to be negligible under atmospheric conditions. S45 can convert into an alkyl radical S46 through the cleavage of C_4-C_5 bond, or dissociate to an alkyl radical S50 via the rupture of C_3-C_4 bond. The barrier of the former reaction is 3.9 kcal/mol, which is lower than that of the latter pathway by 2.6 kcal/mol, indicating that the formation of S46 is kinetically preferable. Then, S46 decomposes into an OH radical byproduct and a C_8-product S47 bearing a –OOH, a peroxide bridge, two carbonyls, and three

https://doi.org/10.5194/egusphere-2025-4646
Preprint. Discussion started: 23 October 2025
© Author(s) 2025. CC BY 4.0 License.

hydroxy groups, which is expected to be the dominant pathway owing to its lower barrier. The rate coefficient k_{RS47} is estimated to be 1.8 × 10^9 s^{-1}, which is about two orders of magnitude greater than the pseudo-first-order rate constant k'_{R+O2} (3.0 × 10^7 s^{-1}). The result reveals that the unimolecular decomposition of S46 is more competitive than the bimolecular reaction with O_2. The formed OH radicals can once again participate in the oxidations of styrene and its highly oxidized products, continuing these processes until they are completely consumed.

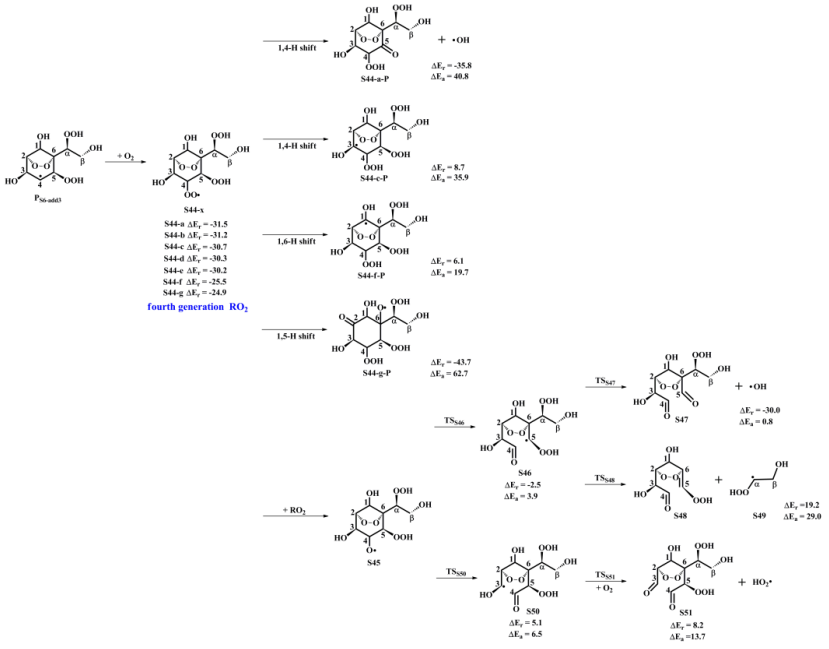

Figure 6. PES for the subsequent reactions of $P_{S6\text{-}add3}$ in the presence of O_2 at the M06-2X/6-311++G(3df,3pd)//M06-2X/6-31+g(d,p) level

3.3.2 The oxidation mechanism of 2nd-$RONO_2$ initiated by OH radicals

A schematic PES for the OH-initiated oxidation of 2nd-$RONO_2$ (S26) is presented in Figure S15. The bimolecular reaction of S26 with OH radicals encompasses four possible routes, namely, $R_{S26\text{-}add3}$, $R_{S26\text{-}add4}$, $R_{S26\text{-}add3'}$ and $R_{S26\text{-}add4'}$. Among these four OH-addition reactions, $R_{S26\text{-}add3}$ has the smallest barrier (ΔE_a = 2.4 kcal/mol), which is in line with the reaction S6 + OH that *syn*-OH-addition reaction occurring at the

https://doi.org/10.5194/egusphere-2025-4646
Preprint. Discussion started: 23 October 2025
© Author(s) 2025. CC BY 4.0 License.

C_3-site is predominant. The *syn*-OH-addition product $P_{S26\text{-}add3}$ has three potential unimolecular decay pathways, as depicted in Figure S16: (1) $P_{S26\text{-}add3}$ dissociates to an epoxide S52 and a NO_2 molecule through a cyclization process (ΔE_a = 18.5 kcal/mol); (2) $P_{S26\text{-}add3}$ isomerizes to an alkyl radical S53 via the intramolecular 1,2 H-shift (ΔE_a = 40.0 kcal/mol); (3) $P_{S26\text{-}add3}$ converts into an alkene S54 via the elimination of hydrogen atom (ΔE_a = 39.1 kcal/mol). Based on the values of ΔE_a, the dominant pathway of the unimolecular decomposition of $P_{S26\text{-}add3}$ is the formation of S52. The rate coefficient k_{R52} is calculated to be 0.4 s^{-1}, which is about seven orders of magnitude lower than the pseudo-first-order rate constant k'_{R+O2}, indicating that the unimolecular decomposition of $P_{S26\text{-}add3}$ is less importance.

In the presence of O_2, $P_{S26\text{-}add3}$ can react with an O_2 molecule leading to the formation of the fourth generation peroxy radicals S55-x, which has seven possible conformers, as shown in Figure 7. For the intramolecular H-shifts of S55-x, not all of reactants (S55-c, S55-d and S55-e) have the suitable conformers that allow for the pathways across the reaction barriers. The barriers of intramolecular H-shifts are considerably high (ΔE_a = 20.8 kcal/mol), making them uncompetitive in the atmosphere. Alternatively, S55-x can react with other RO_2 radicals forming an alkoxyl radical S56, followed by decomposition into an alkyl radical S57 via the breakage of C_4-C_5 bond (ΔE_a = 2.0 kcal/mol), or fragmentation into an alkyl radical S61 through the cleavage of C_3-C_4 bond (ΔE_a = 4.5 kcal/mol). The aforementioned results reveal that the formation of S57 is energetically favorable, which is consistent with the conclusion derived from the unimolecular decomposition of S45 that the breakage of C_4-C_5 bond is feasible. Next, S57 dissociates to a NO_2 coproduct and a C_8-product S58 that possessed a $-NO_3$, a peroxide bridge, two carbonyls, and three hydroxy groups. This pathway is expected to be the dominant one (ΔE_a = 1.5 kcal/mol), with the rate coefficient k_{RS58} of 1.2 × 10^9 s^{-1}. The resulting NO_2 can further participate in the cycling of NO_x, ultimately generating tropospheric ozone and SOA.

https://doi.org/10.5194/egusphere-2025-4646
Preprint. Discussion started: 23 October 2025
© Author(s) 2025. CC BY 4.0 License.

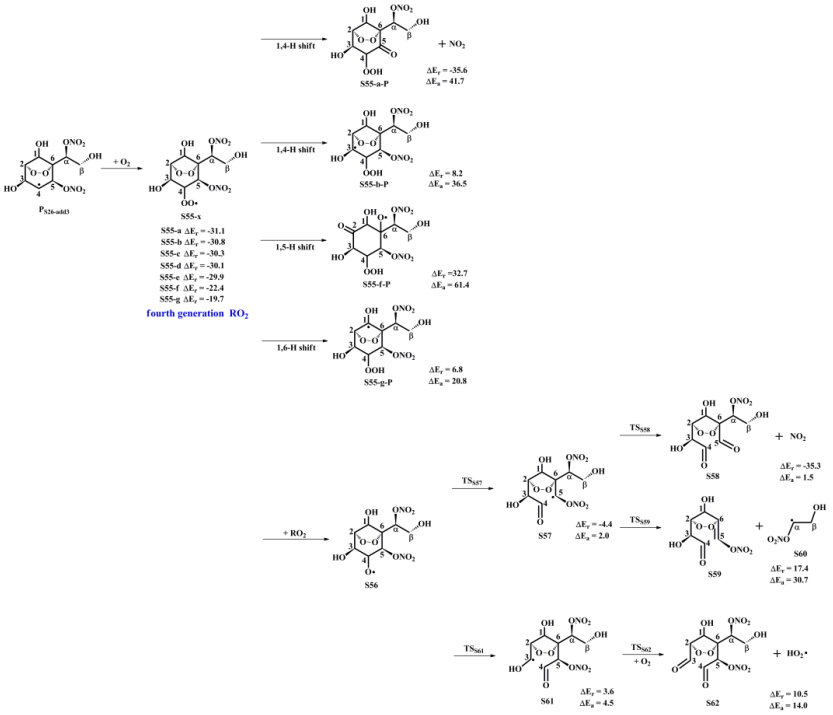

Figure 7. PES for the subsequent reactions of $P_{S26\text{-}add3}$ in the presence of O_2 at the M06-2X/6-311++G(3df,3pd)//M06-2X/6-31+g(d,p) level

3.4 Volatility

The saturated vapour pressure (P^0) and saturated concentration (c^0) of styrene and its multi-generation OH oxidation closed-shell products are predicted by using the SIMPOL.1 method (Pankow et al., 2008), and the results are listed in Table S6. The P^0 and C^0 of styrene are estimated to be 4.63 × 10^{-3} atm and 1.95 × 10^7 ug/m^3, respectively, which are 4-5 orders of magnitude greater than those of the first generation products S4 and S5. Based on the Volatility Basis Set (VBS) of organic compounds as proposed by Donahue et al., (2012) S4 and S5 are classified as intermediate volatility organic compounds (IVOCs), which exist exclusively in the gas phase under atmospheric conditions (Bianchi et al., 2019). The second generation products mainly include the ring-opening (S10, S12, S14, S20, S23, S32, and S40-1) and ring-retaining species (S6 and S26). Based on the values of c^0, S12, S23 and S32 belong to IVOCs, while S20 and S40-1 belong to semivolatile organic compounds

https://doi.org/10.5194/egusphere-2025-4646
Preprint. Discussion started: 23 October 2025
© Author(s) 2025. CC BY 4.0 License.

(SVOC). The difference in volatility is attributed to the fact that the carbon number and functional group of the former case are significantly lower than those of the latter case. S6 and S26 are classified as low volatility organic compounds (LVOCs), which can condense onto the existing large particles (Bianchi et al., 2019). Notably, the third generation products S47 and S51 are also classified as LVOCs, but their c^0 values are two orders of magnitude lower than those of the second generation product S6. A similar conclusion is also obtained when comparing the c^0 values of the third generation products S58 and S62 with those of the second generation product S26. The aforementioned results reveal that the volatility of the multiple generation ·OH oxidation products significantly decreases with increasing the number of ·OH oxidation steps. As the oxidation reactions of the third generation products proceed further, the formed products may possess sufficiently low volatility to participate in the formation and growth of new aerosol particle.

4 Conclusions

The formation mechanisms of highly oxidized products from the multi-generation ·OH oxidation of styrene under different NO_x conditions are investigated by mean of quantum chemical methods. The primary conclusions are summarized as follows.

(a) For the first generation ·OH oxidation of styrene, the addition of OH radicals to terminal carbon (C_β-site) of a vinyl group is the dominant pathway. For the isomerization of the first generation RO_2 radicals formed in the association reaction of OH-addition product with O_2, it can proceed through intramolecular hydrogen atom transfer from the –OH group to the terminal oxygen atom to form a hydroperoxyalkoxy radical, followed by decomposition into benzaldehyde by the successive elimination of HCHO and OH radicals. The bimolecular reactions of the first generation RO_2 radicals with HO_2 radicals and NO lead to the formation of the first generation closed-shell products 1^{st}-ROOH ($C_8H_{10}O_3$), benzaldehyde (C_7H_6O), and 1^{st}-$RONO_2$ ($C_8H_9NO_3$).

https://doi.org/10.5194/egusphere-2025-4646
Preprint. Discussion started: 23 October 2025
© Author(s) 2025. CC BY 4.0 License.

(b) For the second generation OH oxidation of 1st-ROOH, OH-addition occurring at the opposite direction of –OOH group exhibit significantly lower barriers compared to those at the same direction of –OOH group. The addition of OH radicals to C_1-site has the smallest barrier among the competing OH-addition reactions. BPR formed by two O_2-addition steps and a cyclization process can either react with $RO_2\cdot$ and NO to produce BAR, or interact with $HO_2\cdot$ and NO to form the second generation closed-shell products 2nd-ROOH ($C_8H_{12}O_8$) and 2nd-$RONO_2$ ($C_8H_{10}N_2O_{10}$). The formed BAR may undergo via the ring-opening and subsequent decomposition reactions to generate an unsaturated 1,4-dicarbonyl compound $C_4H_4O_2$, a ketene-enol $C_4H_4O_2$, and a hydroperoxide $C_4H_6O_5$ bearing a hydroxyl and two carbonyl groups. Alternatively, it can proceed through the cyclization and subsequent dissociation reactions to produce a glycolaldehyde and a epoxide $C_6H_6O_5$ containing a hydroxy and three carbonyl groups. The branching ratios of these two pathways are 74.7% and 25.3%, respectively.

(c) For the second generation OH oxidation of 1st-$RONO_2$, the OH-addition reaction at the C1-site, which proceeds in the opposite direction as the $–ONO_2$ group, has the smallest barrier. BAR formed in the reactions of BPR with HO_2 radicals and NO can proceed either the ring opening or cyclization process to from alkyl radicals S27 and S35, with the branching ratio of 69.2% and 30.8%. The main products of the decomposition of S27 are an unsaturated 1,4-dicarbonyl compound $C_4H_4O_2$ and an organic nitrate $C_4H_5NO_6$ bearing a hydroxyl and two carbonyl groups. The primary products of the dissociation of S35 are a glyoxal and a C_6-epoxide specie $C_6H_7NO_7$ containing a $–NO_3$, a hydroxyl and two carbonyl groups.

(d) For the third generation OH oxidation of 2nd-ROOH and 2nd-$RONO_2$, *syn*-OH-addition reactions occurring at the C_3-site are predominant. The alkoxyl radical formed in the reaction 2nd-ROOH + OH decomposes into an OH radical byproduct and a C_8-product, $C_8H_{12}O_9$, bearing a –OOH, a peroxide bridge, two carbonyls, and three hydroxy groups. The alkoxyl radical formed in the reaction 2nd-$RONO_2$ + OH dissociates to a NO_2 co-product and a C_8-product, $C_8H_{11}NO_{10}$, containing a $–NO_3$, a peroxide bridge, two carbonyls, and three hydroxy groups.

https://doi.org/10.5194/egusphere-2025-4646
Preprint. Discussion started: 23 October 2025
© Author(s) 2025. CC BY 4.0 License.

(e) The first generation products 1^{st}-ROOH and 1^{st}-$RONO_2$ belong to IVOCs, which exist exclusively in the gas phase. In the numerous second generation products, only 2^{nd}-ROOH and 2^{nd}-$RONO_2$ are identified as IVOCs. Although the third generation products are also classified as LVOC, their c^0 values are several orders of magnitude lower than those of the second generation products. As a result, the volatility of the multiple generation ·OH oxidation products significantly decreases with increasing the number of ·OH oxidation steps.

Data availability

The data are accessible by contacting the corresponding author (huangyu@ieecas.cn).

Supplement

Tables S1, S2 and S4 list the relative electronic energy, free energy and Boltzmann population of different conformers involved in S2-1-x, S8-x and S28-x. Tables S3 and S5 list the MC-TST rate coefficients for the intramolecular H-shift reactions of S8-x and S28-x. Table S6 summaries the saturated vapour pressure and saturated concentrations of styrene and its multiple generation ·OH oxidation closed-shell products. Figures S1-S3 display the PESs for the unimolecular reactions of S2-2-x, S2-3-x and S2-4-x. Figure S4 shows the global minimum structures of 1^{st}-ROOH(S4) and 1^{st}-$RONO_2$(S5). Figures S5 and S9 show the PESs for the addition reactions $P_{S4\text{-}add1}$ + O_2 and $P_{S5\text{-}add1}$ + O_2, and their subsequent intramolecular cyclization reactions. Figures S6 and S10 present the lowest energy conformers of third generation peroxy radical $P_{S4\text{-}add1''}$-OO-a-2 and $P_{S5\text{-}add1''}$-OO-a-2. Figures S7-S8 depict the PESs for the intramolecular hydrogen transfer reactions of S8-x and S16-x. Figures S11 and S12 display the PESs for the intramolecular hydrogen transfer reactions of S28-x and S36-x. Figures S13 and S14 show the PESs for the ·OH-initiated oxidation of 2^{nd}-ROOH (S6) and unimolecular decomposition of $P_{S6\text{-}add3}$.

https://doi.org/10.5194/egusphere-2025-4646
Preprint. Discussion started: 23 October 2025
© Author(s) 2025. CC BY 4.0 License.

Figures S15 and S16 show the PESs for the OH-initiated oxidation of 2^{nd}-$RONO_2$ (S26) and unimolecular decomposition of $P_{S26\text{-}add3}$.

Author contribution

LC and YH conceptualized the study. LC conducted quantum chemical calculation. YX and ZJ analyzed the data. LC conducted the volatility estimation. All authors discussed the results and commented on the manuscript.

Competing interests

The contact author has declared that none of the authors has any competing interests.

Financial support

This study was supported by the National Natural Science Foundation of China (grant nos. 42175134) and the Youth Innovation Promotion Association of the Chinese Academy of Sciences (grant nos. 2022415).

Reference

Alecu, I. M., Zheng, J., Zhao, Y., and Truhlar, D. G.: Computational thermochemistry: scale factor databases and scale factors for vibrational frequencies obtained from electronic model chemistries, J. Chem. Theory Comput., 6, 2872-2887, https://doi.org/10.1021/ct100326h, 2010.

Bianchi, F., Kurtén, T., Riva, M., Mohr, C., Rissanen, M. P., Roldin, P., Berndt, T., Crounse, J. D., Wennberg, P. O., Mentel, T. F., Wildt, J., Junninen, H., Jokinen, T., Kulmala, M., Worsnop, D. R., Thornton, J. A., Donahue, N., Kjaergaard, H. G., and Ehn, M.: Highly oxygenated organic molecules (HOM) from gas-phase autoxidation involving peroxy radicals: a key contributor to atmospheric aerosol, Chem. Rev., 119, 3472-3509, https://doi.org/10.1021/acs.chemrev.8b00395, 2019.

Bloss, C., Wagner, V., Jenkin, M. E., Volkamer, R., Bloss, W. J., Lee, J. D., Heard, D. E., Wirtz, K., Martin-Reviejo, M., Rea, G., Wenger, J. C., and Pilling, M. J.: Development of a detailed chemical mechanism (MCMv3.1) for the atmospheric oxidation of aromatic hydrocarbons, Atmos. Chem. Phys., 5, 641-664, https://doi.org/10.5194/acp-5-641-2005, 2005.

Cabrera-Perez, D., Taraborrelli, D., Sander, R., and Pozzer, A.: Global atmospheric budget of simple monocyclic aromatic compounds, Atmos. Chem. Phys., 16, 6931-6947, https://doi.org/10.5194/acp-16-6931-2016, 2016.

https://doi.org/10.5194/egusphere-2025-4646
Preprint. Discussion started: 23 October 2025
© Author(s) 2025. CC BY 4.0 License.

Canneaux, S., Bohr, F., and Henon, E.: KiSThelP: a program to predict thermodynamic properties and rate constants from quantum chemistry results, J. Comput. Chem., 35, 82-93, https://doi.org/10.1002/jcc.23470, 2013.

Chen, L., Huang, Y., Xue, Y., Jia, Z., and Wang, W.: Atmospheric oxidation of 1-butene initiated by OH radical: Implications for ozone and nitrous acid formations, Atmos. Environ., 244, 118010-118021, https://doi.org/10.1016/j.atmosenv.2020.118010, 2021.

Cho, J., Roueintan, M., and Li, Z.: Kinetic and dynamic investigations of OH reaction with styrene, J. Phys. Chem. A, 118, 9460-9470, https://doi.org/10.1021/jp501380j, 2014.

Donahue, N. M., Kroll, J. H., Pandis, S. N., and Robinson, A. L.: A two-dimensional volatility basis set – Part 2: Diagnostics of organic-aerosol evolution, Atmos. Chem. Phys., 12, 615-634, https://doi.org/10.5194/acp-12-615-2012, 2012.

Eckart, C.: The penetration of a potential barrier by electrons, Phys. Rev., 35, 1303-1309, https://doi.org/10.1103/PhysRev.35.1303, 1930.

Environmental Protection Agency (EPA). Clean Air Act: Title I-Air Pollution Prevention and Control. U.S. 1990.

Fernández-Ramos, A., Ellingson, B. A., Meana-Pañeda, R., Marques, J. M. C., and Truhlar, D. G.: Symmetry numbers and chemical reaction rates, Theor. Chem. Acc., 118, 813-826, https://doi.org/10.1007/s00214-007-0328-0, 2007.

Forstner, H. J. L., Flagan, R. C., and Seinfeld, J. H.: Secondary organic aerosol from the photooxidation of aromatic hydrocarbons: molecular composition, Environ. Sci. Technol., 31, 1345-1358, https://doi.org/10.1021/es9605376, 1997.

Frisch, M. J., Trucks, G. W., Schlegel, H. B., Scuseria, G. E., Robb, M. A., Cheeseman, J. R., Scalmani, G., Barone, V., Petersson, G. A., Nakatsuji, H., Li, X., Caricato, M., Marenich, A. V., Bloino, J., Janesko, B. G., Gomperts, R., Mennucci, B., Hratchian, H. P., Ortiz, J. V., Izmaylov, A. F., Sonnenberg, J. L., Williams-Young, D., Ding, F., Lipparini, F., Egidi, F., Goings, J., Peng, B., Petrone, A., Henderson, T., Ranasinghe, D., Zakrzewski, V. G., Gao, J., Rega, N., Zheng, G., Liang, W., Hada, M., Ehara, M., Toyota, K., Fukuda, R., Hasegawa, J., Ishida, M., Nakajima, T., Honda, Y., Kitao, O., Nakai, H., Vreven, T., Throssell, K., Montgomery, J. A., Peralta, J. J. E., Ogliaro, F., Bearpark, M. J., Heyd, J. J., Brothers, E. N., Kudin, K. N., Staroverov, V. N., Keith, T. A., Kobayashi, R., Normand, J., Raghavachari, K., Rendell, A. P., Burant, J. C., Iyengar, S. S., Tomasi, J., Cossi, M., Millam, J. M., Klene, M., Adamo, C., Cammi, R., Ochterski, J. W., Martin, R. L., Morokuma, K., Farkas, O., Foresman, J. B., and Fox, D. J.: Gaussian 16, Revision B.01, Gaussian, Inc., Wallingford CT, 2016.

Fu, Z., Guo, S., Xie, H. B., Zhou, P., Boy, M., Yao, M., and Hu, M.: A near-explicit reaction mechanism of chlorine-initiated limonene: implications for health risks associated with the concurrent use of cleaning agents and disinfectants, Environ. Sci. Technol., 58, 19762-19773, https://doi.org/10.1021/acs.est.4c04388, 2024.

Fu, Z., Ma, F., Liu, Y., Yan, C., Huang, D., Chen, J., Elm, J., Li, Y., Ding, A., Pichelstorfer, L., Xie, H. B., Nie, W., Francisco, J. S., and Zhou, P.: An overlooked oxidation mechanism of toluene: computational predictions and experimental validations, Chem. Sci., 14, 13050-13059, https://doi.org/10.1039/D3SC03638C, 2023.

Fu, Z., Xie, H. B., Elm, J., Guo, X., Fu, Z., and Chen, J.: Formation of low-volatile products and unexpected high formaldehyde yield from the atmospheric oxidation of methylsiloxanes, Environ. Sci. Technol., 54, 7136-7145, https://doi.org/10.1021/acs.est.0c01090, 2020.

https://doi.org/10.5194/egusphere-2025-4646
Preprint. Discussion started: 23 October 2025
© Author(s) 2025. CC BY 4.0 License.

Fukui, K.: The path of chemical reactions - the IRC approach, Acc. Chem. Res., 14, 363-368, https://doi.org/10.1021/ar00072a001, 1981.

Garmash, O., Rissanen, M. P., Pullinen, I., Schmitt, S., Kausiala, O., Tillmann, R., Zhao, D., Percival, C., Bannan, T. J., Priestley, M., Hallquist, Å M., Kleist, E., Kiendler-Scharr, A., Hallquist, M., Berndt, T., McFiggans, G., Wildt, J., Mentel, T. F., and Ehn, M.: Multi-generation OH oxidation as a source for highly oxygenated organic molecules from aromatics, Atmos. Chem. Phys., 20, 515-537, https://doi.org/10.5194/acp-20-515-2020, 2020.

Gilbert, R. G., and Smith, S. C.: Theory of unimolecular and recombination reactions, Blackwell Scientific: Carlton, Australia, 1990.

Glowacki, D. R., Liang, C. H., Morley, C., Pilling, M. J., and Robertson, S. H.: MESMER: an open-source master equation solver for multi-energy well reactions, J. Phys. Chem. A, 116, 9545-9560, https://doi.org/10.1021/jp3051033, 2012.

Holbrook, K. A., Pilling, M. J., Robertson, S. H., and Robinson, P. J.: Unimolecular reactions, 2nd ed.; Wiley: New York, 1996.

Huang, Y., Su, T., Wang, L., Wang, N., Xue, Y., Dai, W., Lee, S. C., Cao, J., and Ho, S. S. H.: Evaluation and characterization of volatile air toxics indoors in a heavy polluted city of northwestern China in wintertime, Sci. Total Environ., 662, 470-480, https://doi.org/10.1016/j.scitotenv.2019.01.250, 2019.

Hyttinen, N., Kupiainen-Määttä, O., Rissanen, M. P., Muuronen, M., Ehn, M., and Kurtén, T.: Modeling the charging of highly oxidized cyclohexene ozonolysis products using nitrate-based chemical ionization, J. Phys. Chem. A, 119, 6339-6345, https://doi.org/10.1021/acs.jpca.5b01818, 2015.

Iuga, C., Galano, A., and Vivier-Bunge, A.: Theoretical investigation of the OH-initiated oxidation of benzaldehyde in the troposphere, Chem. Phys. Chem., 9, 1453-1459, https://doi.org/10.1002/cphc.200800144, 2008.

Iyer, S., Kumar, A., Savolainen, A., Barua, S., Daub, C., Pichelstorfer, L., Roldin, P., Garmash, O., Seal, P., Kurtén, T., and Rissanen, M.: Molecular rearrangement of bicyclic peroxy radicals is a key route to aerosol from aromatics, Nat. Commun., 14, 4984-4991, https://doi.org/10.1038/s41467-023-40675-2, 2023.

Ji, Y., Zhao, J., Terazono, H., Misawa, K., Levitt, N. P., Li, Y., Lin, Y., Peng, J., Wang, Y., Duan, L., Pan, B., Zhang, F., Feng, X., An, T., Marrero-Ortiz, W., Secrest, J., Zhang, A. L., Shibuya, K., Molina, M. J., and Zhang, R.: Reassessing the atmospheric oxidation mechanism of toluene, Proc. Natl. Acad. Sci. U.S.A., 114, 8169-8174, https://doi.org/10.1073/pnas.1705463114, 2017.

Ji, Y., Zheng, J., Qin, D., Li, Y., Gao, Y., Yao, M., Chen, X., Li, G., An, T., and Zhang, R.: OH-initiated oxidation of acetylacetone: implications for ozone and secondary organic aerosol formation, Environ. Sci. Technol., 52, 11169-11177, https://doi.org/10.1021/acs.est.8b03972, 2018.

Koppmann, R.: Volatile organic compounds in the atmosphere, John Wiley & Sons, 2008.

Li, M., Zhang, Q., Zheng, B., Tong, D., Lei, Y., Liu, F., Hong, C., Kang, S., Yan, L., Zhang, Y., Bo, Y., Su, H., Cheng, Y., and He, K.: Persistent growth of anthropogenic non-methane volatile organic compound (NMVOC) emissions in China during 1990-2017: drivers, speciation and ozone formation potential, Atmos. Chem. Phys., 19, 8897-8913, https://doi.org/10.5194/acp-19-8897-2019, 2019.

https://doi.org/10.5194/egusphere-2025-4646
Preprint. Discussion started: 23 October 2025
© Author(s) 2025. CC BY 4.0 License.

749 Lu, T.: Molclus program, Version 1.9.3. http://www.keinsci.com/research/molclus.html (accessed
750 May 21, 2024).
751 Ma, F., Guo, X., Xia, D., Xie, H. B., Wang, Y., Elm, J., Chen, J., and Niu, J.: Atmospheric
752 chemistry of allylic radicals from isoprene: a successive cyclization-driven autoxidation
753 mechanism, Environ. Sci. Technol., 55, 4399-4409, https://doi.org/10.1021/acs.est.0c07925,
754 2021.
755 Møller, K. H., Berndt, T., and Kjaergaard, H. G.: Atmospheric autoxidation of amines, Environ.
756 Sci. Technol., 54, 11087-11099, https://doi.org/10.1021/acs.est.0c03937, 2020.
757 Møller, K. H., Otkjær, R. V., Hyttinen, N., Kurtén, T., and Kjaergaard, H. G.: Cost-effective
758 implementation of multiconformer transition state theory for peroxy radical hydrogen shift
759 reactions, J. Phys. Chem. A, 120, 10072-10087, https://doi.org/10.1021/acs.jpca.6b09370,
760 2016.
761 Molteni, U., Bianchi, F., Klein, F., Haddad, I. E., Frege, C., Rossi, M. J., Dommen, J., and
762 Baltensperger, U.: Formation of highly oxygenated organic molecules from aromatic
763 compounds, Atmos. Chem. Phys., 18, 1909-1921, https://doi.org/10.5194/acp-18-1909-2018,
764 2018.
765 Ng, N. L., Kroll, J. H., Chan, A. W. H., Chhabra, P. S., Flagan, R. C., and Seinfeld, J. H.:
766 Secondary organic aerosol formation from m-xylene, toluene, and benzene, Atmos. Chem.
767 Phys., 7, 3909-3922, https://doi.org/10.5194/acp-7-3909-2007, 2007.
768 Nie, W., Yan, C., Huang, D. D., Wang, Z., Liu, Y., Qiao, X., Guo, Y., Tian, L., Zheng, P., Xu, Z., Li,
769 Y., Xu, Z., Qi, X., Sun, P., Wang, J., Zheng, F., Li, X., Yin, R., Dallenbach, K. R., Bianchi, F.,
770 Petäjä, T., Zhang, Y., Wang, M., Schervish, M., Wang, S., Qiao, L., Wang, Q., Zhou, M.,
771 Wang, H., Yu, C., Yao, D., Guo, H., Ye, P., Lee, S., Li, Y. J., Liu, Y., Chi, X., Kerminen, V. M.,
772 Ehn, M., Donahue, N. M., Wang, T., Huang, C., Kulmala, M., Worsnop, D, Jiang, J., and
773 Ding, A.: Secondary organic aerosol formed by condensing anthropogenic vapours over
774 China's megacities, Nat. Geosci., 15, 255-261, https://doi.org/10.1038/s41561-022-00922-5,
775 2022.
776 Pankow, J. F., and Asher, W. E.: SIMPOL.1: a simple group contribution method for predicting
777 vapor pressures and enthalpies of vaporization of multifunctional organic compounds, Atmos.
778 Chem. Phys., 8, 2773-2796, https://doi.org/10.5194/acp-8-2773-2008, 2008.
779 Pasik, D., Frandsen, B. N., Meder, M., Iyer, S., Kurtén, T., and Myllys, N.: Gas-phase oxidation of
780 atmospherically relevant unsaturated hydrocarbons by acyl peroxy radicals, J. Am. Chem.
781 Soc., 146, 13427-13437, https://doi.org/10.1021/jacs.4c02523, 2024.
782 Rissanen, M. P., Kurtén, T., Sipilä, M., Thornton, J. A., Kangasluoma, J., Sarnela, N., Junninen, H.,
783 Jørgensen, S., Schallhart, S., Kajos, M. K., Taipale, R., Springer, M., Mentel, T. F.,
784 Ruuskanen, T., Petäjä, T., Worsnop, D. R., Kjaergaard, H. G., and Ehn, M.: The formation of
785 highly oxidized multifunctional products in the ozonolysis of cyclohexene, J. Am. Chem.
786 Soc., 136, 15596-15606, https://doi.org/10.1021/ja507146s, 2014.
787 Sebbar, N., Bozzelli, J. W., and Bockhorn, H.: Thermochemistry and reaction paths in the
788 oxidation reaction of benzoyl radical: C_6H_5C (=O), J. Phys. Chem. A, 115, 11897-11914,
789 https://doi.org/10.1021/jp2078067, 2011.
790 Shen, H., Vereecken, L., Kang, S., Pullinen, I., Fuchs, H., Zhao, D., and Mentel, T. F.: Unexpected
791 significance of a minor reaction pathway in daytime formation of biogenic highly oxygenated
792 organic compounds, Sci. Adv., 8, eabp8702, https://doi.org/10.1126/sciadv.abp8702, 2022.

https://doi.org/10.5194/egusphere-2025-4646
Preprint. Discussion started: 23 October 2025
© Author(s) 2025. CC BY 4.0 License.

Sun, J., Wu, F., Hu, B., Tang, G., Zhang, J., and Wang, Y.: VOC characteristics, emissions and contributions to SOA formation during hazy episodes, Atmos. Environ., 141, 560-570, https://doi.org/10.1016/j.atmosenv.2016.06.060, 2016.

Tajuelo, M., Bravo, I., Rodríguez, A., Aranda, A., Díaz-de-Mera, Y., and Rodríguez, D.: Atmospheric sink of styrene, α-methylstyrene, trans-β-methylstyrene and indene: Rate constants and mechanisms of Cl atom-initiated degradation, Atmos. Environ., 200, 78-89, https://doi.org/10.1016/j.atmosenv.2018.11.059, 2019c.

Tajuelo, M., Rodríguez, A., Baeza-Romero, M. T., Aranda, A., Díaz-de-Mera, Y., and Rodríguez, D.: Secondary organic aerosol formation from α-methylstyrene atmospheric degradation: Role of NO_x level, relative humidity and inorganic seed aerosol, Atmos. Res., 230, 104631-104640, https://doi.org/10.1016/j.atmosres.2019.104631, 2019b.

Tajuelo, M., Rodríguez, D., Baeza-Romero, M. T., Díaz-de-Mera, Y., Aranda, A., and Rodríguez, A.: Secondary organic aerosol formation from styrene photolysis and photooxidation with hydroxyl radicals, Chemosphere, 231, 276-286, https://doi.org/10.1016/j.chemosphere.2019.05.136, 2019a.

Wang, H., Ji, Y., Gao, Y., Li, G., and An, T.: Theoretical model on the formation possibility of secondary organic aerosol from OH initialed oxidation reaction of styrene in the presence of O_2/NO, Atmos. Environ., 101, 1-9, https://doi.org/10.1016/j.atmosenv.2014.10.042, 2015.

Wang, L., Wu, R., and Xu, C.: Atmospheric oxidation mechanism of benzene. Fates of alkoxy radical intermediates and revised mechanism, J. Phys. Chem. A, 117, 14163-14168, https://doi.org/10.1021/jp4101762, 2013.

Wang, M., Chen, D., Xiao, M., Ye, Q., Stolzenburg, D., Hofbauer, V., Ye, P., Vogel, A. L., Mauldin, R. L., Amorim, A., Baccarini, A., Baumgartner, B., Brilke, S., Dada, L., Dias, A., Duplissy, J., Finkenzeller, H., Garmash, O., He, X. C., Hoyle, C. R., Kim, C., Kvashnin, A., Lehtipalo, K., Fischer, L., Molteni, U., Petäjä, T., Pospisilova, V., Quéléver, L. L. J., Rissanen, M., Simon, M., Tauber, C., Tomé, A., Wagner, A. C., Weitz, L., Volkamer, R., Winkler, P. M., Kirkby, J., Worsnop, D. R., Kulmala, M., Baltensperger, U., Dommen, J., El-Haddad, I., and Donahue, N. M.: Photo-oxidation of aromatic hydrocarbons produces low-volatility organic compounds, Environ. Sci. Technol., 54, 7911-7921, https://doi.org/10.1021/acs.est.0c02100, 2020.

Wang, S., and Li, H.: NO_3-initiated gas-phase formation of nitrated phenolic compounds in polluted atmosphere, Environ. Sci. Technol., 55, 2899-2907, https://doi.org/10.1021/acs.est.0c08041, 2021.

Wang, S., Newland, M. J., Deng, W., Rickard, A. R., Hamilton, J. F., Muñoz, A., Ródenas, M., Vázquez, M. M., Wang, L., and Wang, X.: Aromatic photo-oxidation, a new source of atmospheric acidity, Environ. Sci. Technol., 54, 7798-7806, https://doi.org/10.1021/acs.est.0c00526, 2020.

Wang, S., Wu, R., Berndt, T., Ehn, M., and Wang, L.: Formation of highly oxidized radicals and multifunctional products from the atmospheric oxidation of alkylbenzene, Environ. Sci. Technol., 51, 8442-8449, https://doi.org/10.1021/acs.est.7b02374, 2017.

Wu, R., Pan, S., Li, Y., and Wang, L.: Atmospheric oxidation mechanism of toluene, J. Phys. Chem. A, 118, 4533-4547, https://doi.org/10.1021/jp500077f, 2014.

Wu, X., Hou, Q., Huang, J., Chai, J., and Zhang, F.: Exploring the OH-initiated reactions of styrene in the atmosphere and the role of van der Waals complex, Chemosphere, 282, 131004-131012, https://doi.org/10.1016/j.chemosphere.2021.131004, 2021.

https://doi.org/10.5194/egusphere-2025-4646
Preprint. Discussion started: 23 October 2025
© Author(s) 2025. CC BY 4.0 License.

Wu, X., Huang, C., Niu, S., and Zhang, F.: New theoretical insights into the reaction kinetics of toluene and hydroxyl radicals, Phys. Chem. Chem. Phys., 22, 22279-22288, https://doi.org/10.1039/D0CP02984J, 2020.

Xu, L., Møller, K. H., Crounse, J. D., Kjaergaard, H. G., and Wennberg, P. O.: New insights into the radical chemistry and product distribution in the OH-initiated oxidation of benzene, Environ. Sci. Technol., 54, 13467-13477, https://doi.org/10.1021/acs.est.0c04780, 2020.

Yan, Y., Cabrera-Perez, D., Lin, J., Pozzer, A., Hu, L., Millet, D. B., Porter, W. C., and Lelieveld, J.: Global tropospheric effects of aromatic chemistry with the SAPRC-11 mechanism implemented in GEOS-Chem version 9-02, Geosci. Model Dev., 12, 111-130, https://doi.org/10.5194/gmd-12-111-2019, 2019.

Yu, S., Jia, L., Xu, Y., and Pan, Y.: Formation of extremely low-volatility organic compounds from styrene ozonolysis: Implication for nucleation, Chemosphere, 305, 135459-135467, https://doi.org/10.1016/j.chemosphere.2022.135459, 2022.

Yu, S., Jia, L., Xu, Y., and Pan, Y.: Molecular composition of secondary organic aerosol from styrene under different NO_x and humidity conditions, Atmos. Res., 266, 105950-10604, https://doi.org/10.1016/j.atmosres.2021.105950, 2022.

Zaytsev, A., Koss, A. R., Breitenlechner, M., Krechmer, J. E., Nihill, K. J., Lim, C. Y., Rowe, J. C., Cox, J. L., Moss, J., Roscioli, J. R., Canagaratna, M. R., Worsnop, D. R., Kroll, J. H., and Keutsch, F. N.: Mechanistic study of the formation of ring-retaining and ring-opening products from the oxidation of aromatic compounds under urban atmospheric conditions, Atmos. Chem. Phys., 19, 15117-15129, https://doi.org/10.5194/acp-19-15117-2019, 2019.

Zhang, H., Wang, J., Dong, B., Xu, F., Liu, H., Zhang, Q., Zong, W., and Shi, X.: New mechanism for the participation of aromatic oxidation products in atmospheric nucleation, Sci. Total Environ., 917, 170487-170494, https://doi.org/10.1016/j.scitotenv.2024.170487, 2024.

Zhang, R. M., Truhlar, D. G., and Xu, X.: Kinetics of the toluene reaction with OH radical, Research, 2019, Article ID 5373785, https://doi.org/10.34133/2019/5373785, 2019.

Zhao, H., Zhang, Y., Zhao, Q., Li, Y., and Huang, Z.: A theoretical study of H-abstractions of benzaldehyde by H, $O^3(P)$, $^3O_2$, OH, HO_2, and CH_3 radicals: Ab initio rate coefficients and their uncertainty quantification, J. Phys. Chem. A, 126, 7523-7533, https://doi.org/10.1021/acs.jpca.2c02384, 2022.

Zhao, Y., and Truhlar, D. G.: The M06 suite of density functionals for main group thermochemistry, thermochemical kinetics, noncovalent interactions, excited states, and transition elements: two new functionals and systematic testing of four M06-class functionals and 12 other functionals, Theor. Chem. Acc., 120, 215-241, https://doi.org/10.1007/s00214-007-0310-x, 2008.